NeuroImage 325 (2026) 121666

Contents lists available at ScienceDirect

NeuroImage

journal homepage: www.elsevier.com/locate/ynimg

Immediate TMS-EEG responses reveal motor cortex excitability

Antonietta Stango [a,1], Agnese Zazio [a,1], Guido Barchiesi [b], Natale Salvatore Bonfiglio [c], Elisa Dognini [a], Eleonora Marcantoni [d], Marta Bortoletto [a,e,*]

[a] Neurophysiology Lab, IRCCS Istituto Centro San Giovanni di Dio Fatebenefratelli, Brescia, Italy
[b] Cognition in Action (CIA) Unit – PHILAB, Department of Philosophy, Università degli Studi di Milano, Milano, Italy
[c] Statistical service, IRCCS Istituto Centro San Giovanni di Dio Fatebenefratelli, Brescia, Italy
[d] Center for Cognitive Neuroimaging, School of Neuroscience and Psychology, University of Glasgow, Glasgow, United Kingdom
[e] MoMiLab, IMT School for Advanced Studies Lucca, Lucca, Italy

ARTICLE INFO

Keywords:
Primary motor cortex
Cortical excitability
i-TEPs
i-TRP
Source localization

ABSTRACT

The combination of transcranial magnetic stimulation and electroencephalography (TMS-EEG) is typically used to probe cortical excitability at the network level, as local excitability measures were previously not feasible. However, a recent study revealed immediate TMS-evoked potentials (i-TEPs) following primary motor cortex (M1) stimulation, yet their physiological origin remains uncertain. Here, we aimed to test whether this immediate activity is replicable, physiological, and related to motor cortex excitability.

Analyses were conducted on data from 28 healthy participants who underwent M1 stimulation using two opposite biphasic current directions. We run a minimal preprocessing and then, upon visual inspection, we divided the sample according to the presence/absence of muscle artifacts (Muscle/NoMuscle groups). First, we successfully replicated i-TEPs for both current directions. Second, source localization revealed that the i-TEPs signal originated in the precentral gyrus of the stimulated hemisphere. Third, we computed the immediate TMS-related power (i-TRP) to disentangle the components contributing to the i-TEP signal. Two oscillatory peaks emerged at 100–200 Hz and 600–800 Hz. Finally, we tested the relationship between i-TRP components and motor evoked potentials (MEPs) amplitude in NoMuscle groups ($n = 8$ for both current directions, $n = 14$ for anterior-to-posterior and posterior-to-anterior induced current). The analysis showed a robust positive association between i-TRP in the 600–800 Hz range and MEP amplitude, suggesting that this component reflects M1 excitability.

Overall, our findings converge in indicating the physiological nature of immediate TMS-EEG responses, suggesting that they reflect the excitability of the stimulated cortex.

1. Introduction

Assessing the excitability of specific cortical areas is essential for understanding brain dynamics and its impact on behavior, both in healthy populations as well as in patients with neuropsychiatric disorders (Tremblay et al., 2019; Farzan, 2024). To this aim, the combination of transcranial magnetic stimulation and electroencephalography (TMS-EEG) has shown promise by allowing direct manipulation and tracking of neuronal activity in a timely and non-invasive manner. Nevertheless, currently available TMS-EEG measures, including both TMS-evoked potentials (TEPs) (Ilmoniemi et al., 1997) and TMS-related power (TRP, also called event-related spectral perturbation; the acronym TRP was introduced to specifically denote TMS-induced spectral responses, in analogy to TEPs for TMS-evoked potentials) (Rosanova et al., 2009) capture activity from broad networks rather than local responses, and the contribution of recurrent cortical connections complicates the interpretation of the effects of the stimulation (Momi et al., 2021; Massimini et al., 2005; Ozdemir et al., 2020; Bortoletto et al., 2015). Therefore, the complex cortical responses that are recorded after TMS derive from a mixture of local dynamics, more prominent in the early components, and recurrent re-entrant activity (Momi et al., 2023). A local immediate response to stimulation, which most likely occurs in the first milliseconds after the TMS pulse, has yet to be validated as the EEG signal is covered by several artifacts (Hernandez-Pavon et al.,

* Corresponding author at: MoMiLab, IMT School for Advanced Studies Lucca, Lucca, Italy.
E-mail address: marta.bortoletto@imtlucca.it (M. Bortoletto).
[1] Equal contribution.

https://doi.org/10.1016/j.neuroimage.2025.121666
Received 3 July 2025; Received in revised form 7 November 2025; Accepted 18 December 2025
Available online 19 December 2025

2023), and it is typically removed during off-line signal preprocessing (Veniero et al., 2009). A direct measure of cortical excitability would open new avenues for TMS applications in both basic and clinical research. In cognitive neuroscience, it would strengthen causal inferences between specific brain regions and cognitive functions by minimizing the confounding influence of remote regions in the causal chain (Bergmann and Hartwigsen, 2021). In clinical contexts, such a measure could help optimize TMS-based treatments by providing a more accurate method for determining stimulation intensity, an issue that remains unresolved outside the motor cortex (Numssen et al., 2024). Furthermore, tracking cortical excitability could enable real-time monitoring of treatment effects, ultimately leading to more personalized and adaptive stimulation protocols.

In a recent paper (Beck et al., 2024), the EEG signal was recovered at approximately 2 ms after the TMS pulse and revealed new TEP components occurring before 6 ms. These immediate TEP components (i-TEPs) included high-frequency activity resembling the corticospinal descending volleys recorded within the spinal cord (i.e., I-waves), as their amplitude was modulated both by the current direction and by the intensity of the TMS. The authors suggested that these components may reflect a local response of the stimulated cortex. However, the effect of the current direction on I-waves for biphasic stimulation has not been directly tested (Di Lazzaro et al., 2001; Ziemann, 2020), and the effect of the intensity of stimulation, although reported for I-waves (Burke et al., 1993; Kaneko et al., 1996; Di Lazzaro et al., 1999), does not fully rule out the possibility that i-TEPs reflect artifactual activity (e.g., the muscle artifact).

Intrigued by the possibility of developing a novel noninvasive measure for testing local excitability, in the present study we aimed to comprehensively understand the origin of the immediate TMS-EEG responses. First, we aimed to confirm the recent findings on i-TEPs, i.e., to record the i-TEPs both for biphasic AP-PA and for the PA-AP current direction, with a different TMS-EEG system. Second, we aimed to clarify whether immediate TMS-EEG responses have a cortical or an artifactual origin, controlling for the contribution of muscle artifacts. Finally, we calculated the immediate TRP (i-TRP) in high-frequency bands as the TMS-induced event-related spectral perturbation that includes both evoked and induced activity, and we tested its relationship with a typical peripheral measure of cortico-spinal excitability, i.e., motor-evoked potentials (MEPs).

2. Methods

2.1. Main experiment

2.1.1. Participants

The data presented in this paper were collected at the Neurophysiology Laboratory of the IRCCS Istituto Centro San Giovanni di Dio Fatebenefratelli (local ethics committee reference number: 102–2021) and are part of the dataset published in the work by Guidali et al. (2023). The dataset can be found at https://gin.g-node.org/Giacomo_Guidali/Guidali_et_al_2023_EJN_RR. Twenty-eight right-handed participants aged 18 to 50 years completed the study, with a stimulation intensity below 90 % of the maximal stimulator output (MSO) in all conditions.

2.1.2. Data acquisition

The EEG and Electromyographic (EMG) data were acquired using a DC coupled TMS-compatible EEG system (g.HIamp multichannel amplifier, g.tec medical engineering GmbH) with input voltage of ±250 mV (24-bit resolution), a sampling rate of 9.6 kHz and factory implemented hardware filter settings. EEG signals were recorded from 74 electrodes (EasyCap, Brain Products GmbH, Munich, Germany) placed on the scalp according to the 10–10 international system and referenced to FPz. The ground was placed on the tip of the nose. The skin-electrode impedance was maintained below 5 kΩ. EMG signals were recorded from the right abductor pollicis brevis using a bipolar belly tendon montage.

As shown by data from our laboratory (Guidali et al., 2023; Zazio et al., 2022) and a previous study by Freche et al. (2018), these setting allow to reliably record EEG signals as early as 2 ms after the TMS pulse, even in case of EEG amplifier saturation during the TMS pulse. The TMS artifact ends within 1 ms, and then it is followed by a decay artifact that ends within 2 ms when using passive electrodes with an impedance below 5 kΩ, as in this case (Stango et al., 2025).

The original study included three current directions for both monophasic and biphasic pulse waveforms; however, following Beck et al. (2024), only biphasic stimulation (Magstim Rapid^2, Magstim, Whitland, UK) was considered. Specifically, the 2 current directions previously reported by Beck *et al.* were considered: AP-PA and PA-AP. For each condition, eighty single TMS pulses were delivered over the left primary motor cortex (M1) at 110 % of the resting motor threshold (rMT), estimated for each current direction separately. Table 1 reports the rMT for each subject and for each condition. Further information can be found in Guidali et al. (2023).

For each TMS pulse, a digital marker was recorded along with the EEG signal, which was used during preprocessing to segment the epochs around the TMS pulse. It should be noted that the EEG signals recorded with the g.tec amplifier show a constant delay of 11 samples (approximately 1.1 ms) relative to the marker when recorded at a sampling rate of 9600 Hz. This delay is introduced by the amplifier due to intrinsic filtering and downsampling of the Analog-to-Digital Converter (ADC) for analog channels. Therefore, 1.1 ms should be subtracted from the reported values to obtain the actual latencies of the TMS artifacts and EEG signals. This adjustment is necessary when comparing our results with Beck et al. (2024); however, the original values are retained here to maintain consistency with Guidali et al. (2023) and the publicly available dataset.

2.1.3. i-TEPs

To obtain i-TEPs, the preprocessing was limited to the following steps: First, the continuous EEG signal was cut in epochs from −500 ms to 500 ms around the TMS pulse and baseline corrected, from –500 ms to −5 ms. These long epochs were suitable for visual inspection of ocular artefacts and were rejected if they contained ocular artifacts and noise. The signal between 0 and 2.8 ms was removed and replaced with zeros. Next, electrodes with decay artifacts were identified and interpolated (Table 1). After cleaning, shorter epochs (−100 ms to 100 ms) were obtained, and a baseline correction was applied in the first 95 ms, i.e., from −100 ms to −5 ms.

EEG data were visually inspected to identify artifacts, particularly in the 2–6 ms window following TMS. Trials and channels were flagged for rejection if they exhibited clear non-physiological patterns, such as flat segments, abrupt voltage shifts, or abnormally persistent signals. Subjects were excluded if artifacts affected channels close to the stimulation hotspot or if more than 50 % of trials were rejected (see Table 1). After this selection, 21 subjects were included in the AP-PA condition, and 25 were included in the PA-AP condition. Finally, the data were averaged to obtain i-TEPs, and for each current direction, the subjects were divided into two groups, i.e., NoMuscle and Muscle, based on the presence of a visible muscle artifact in the averaged signal. Muscle artifacts were identified by visual inspection as MEP-like responses with lateralized topography in the stimulated hemisphere. The NoMuscle groups included 14 subjects in the AP-PA condition and 10 subjects in the PA-AP condition. The Muscle group included 7 subjects in the AP-PA condition and 15 subjects in the PA-AP condition. A total of 8 subjects belonged to the NoMuscle group for both the AP-PA and PA-AP conditions.

Standard TEP preprocessing methods, such as ICA or SSP-SIR–based cleaning, were not applied because they can remove or attenuate the immediate, fast, and high-amplitude components characteristic of i-TEPs (<10 ms).

Table 1
Individual data on rMT, the presence of muscle artifacts, interpolated channels and the number of rejected epochs for both the AP-PA and PA-AP conditions. Missing data refer to cases that were excluded from further analyses because of decay artifacts or noise. Asterisks indicate subjects who were included in the final sample for statistical analysis, as they belonged to the NoMuscle groups for both the AP-PA and PA-AP conditions.

Subj ID	AP-PA				PA-AP			
	Muscle	rMT	Interpolated channels	N Rejected trials	Muscle	rMT	Interpolated channels	N Rejected trials
S01	Y	52.6 %	FP1, FC1, C1	23	Y	64.6 %	FP1, AFz, F1	14
S02	Y	58.6 %	AF7, Fz, FC2, AFz	6	Y	68.2 %	AF7, Fz, I1	1
S04	N	51.2 %	FC1, FP2, AF7	29	-	-	-	-
S05	-	-	-	-	Y	68.8 %	AF8, PO7	43
S06	-	-	-	-	Y	81.5 %	FCz	39
S07	N	67.1 %	AFz, C2, F10, FC4	7	Y	73.3 %	C2, PO3, F3, FC4, AFz, F10, FP2	22
S08	N*	38.9 %	FC1, TP10, F10, FP2	14	N*	41.7 %	TP10, FC1, F10	12
S09	-	-	-	-	Y	74.0 %	FC1, AFz, AF4	4
S11	Y	64.4 %	FC1, PO9, PO7, CP5	7	Y	75.8 %	PO9, FC1, CP5, PO7, AFz, Cz	7
S13	Y	61.5 %	FT10, TP10, T8, TP8, PO8, AFz	15	Y	68.7 %	FT10, TP10, I2, P8, TP9, TP8, PO8, F2, F5	40
S14	N*	53.9 %	PO3, AF7	27	N*	58.9 %	FT10, PO3, AF7, PO9	33
S15	-	-	-	-	Y	79.9 %	I2, PO10, TP9, P4, I1, Iz, P2, TP8, F2	28
S16	N*	50.2 %	Fz, P9, Pz, FCz, F5, FC2, FC1	21	N*	64.9 %	FC1, P9, PO9, PO7, Pz, Fz, CPz, FCz, AF3, F5, FC2, F2	23
S18	N*	53.4 %	F10, F9, TP7, P2, AF3, AFz, Fz, FC3	15	N*	59.6 %	Fz, TP7, FC3, T8, PO9, F9, F10, AF3, AFz	9
S19	N	64.4 %	T7, F9, TP10, F6, P2, FC6	0	Y	75.4 %	F9, AFz, F6, FC6, FP2	4
S20	Y	65.3 %	F4	21	N	57.0 %	F4	6
S25	N*	57.1 %	F9, TP10, FP2, FP1, FT10	12	N*	65.8 %	F9, F8, Fz, AF8, FP1	3
S27	-	-	-	-	Y	80.9 %	F9, FC2, TP7, T8, TP8, TP10, P10, C4, FT10, P9	17
S29	N*	66 %	F5,PO3,FC4,AF7	24	N*	72.4 %	PO3, FC4, TP7, FC1, Fz, FC3, AF7, F5, AF3, F2	12
S30	-	-	-	-	Y	62.9 %	Fz, F1, P10, AFz, F7	3
S31	Y	58.2 %	FT10, AF3, F2, AFz, I2, FC3, P2	28	Y	67.2 %	FT10, AF3, AFz	15
S33	N	60.3 %	C2, CP2, F2, Cz, AFz, CP3, CP1, F1, C5	27	-	-	-	-
S34	N	54.7 %	C2, AFz, FC2, AF8	15	Y	60.6 %	C2, FT9, AF8, FT10, AFz, FC2	8
S36	N*	55.4 %		17	N*	62.1 %	PO3, F2, F1	2
S37	N*	52.9 %	I2, PO7, PO4, FC2	34	N*	49.6 %	I2, PO7, FT10, PO10, FP1, FCz	34
S38	-	-	-	-	-	-	-	-
S39	N	57.4 %	FC1, AF4, T7 FP2, F2, P5, PO7	20	Y	66.9 %	C2, PO7, P5, PO9, AF4, F2	9
S40	Y	49.1 %	T7, FC1, AF3, FCz	33	N	48.8 %	T7, FC1, FCz, AF3	22

2.1.4. *Time-frequency analysis*

A time-frequency analysis was run on single-trial preprocessed data, considering data from −30 ms to +100 ms with respect to the TMS pulse, within a frequency range between 30 and 1000 Hz. Lower frequencies (<30 Hz) were excluded for two main reasons: (i) they are unlikely to contribute to immediate responses within this time window, and (ii) their inclusion would increase temporal smoothing, potentially spreading artifacts related to the TMS pulse. Hanning taper was applied on a frequency-dependent time window consisting of 5 cycles per frequency (sliding in steps = 1 ms), to ensure a balance between stable estimation of high-frequency components (thus reducing spectral smearing) and temporal specificity" (Herrmann et al., 2014). The Fourier-transform data were used to calculate the inter-trial coherence (ITC) (Delorme and Makeig, 2004), while the power data as measure of TRP. After averaging the calculated TRP over all subjects and conditions, we visually inspected the resulting power peaks between 3 and 6 ms in the frequency range and labelled those between 600 and 800 Hz as fast TRP (fi-TRP) and those between 100 and 200 Hz as slow TRP (si-TRP). Output measures consisted of single-trial TRP – similarly previous studies (e.g., Cohen and van Gaal 2014, Almeida et al. 2011) – averaged in the time-frequency range of fi-TRP (i.e., 3–6 ms, 600–800 Hz) and si-TRP (i.e., 3–6 ms, 100–200 Hz), and restricted to C3, which was used

as a standardized approximation of the left M1 hotspot across participants, and the peak activity of both fi-TRP and si-TRP.

2.1.5. MEPs

To calculate MEPs amplitude, continuous EMG between 0 and 3 ms from the TMS pulse was removed and replaced by an array computed resulting from a cubic interpolation. Then, EMG signal was bandpass-filtered between 10 and 2500 Hz, notch-filtered at 50 Hz (FIR filtering) and epoched from −200 ms to 500 ms with respect to the TMS pulse. Epochs containing muscular or background noise, as indicated by

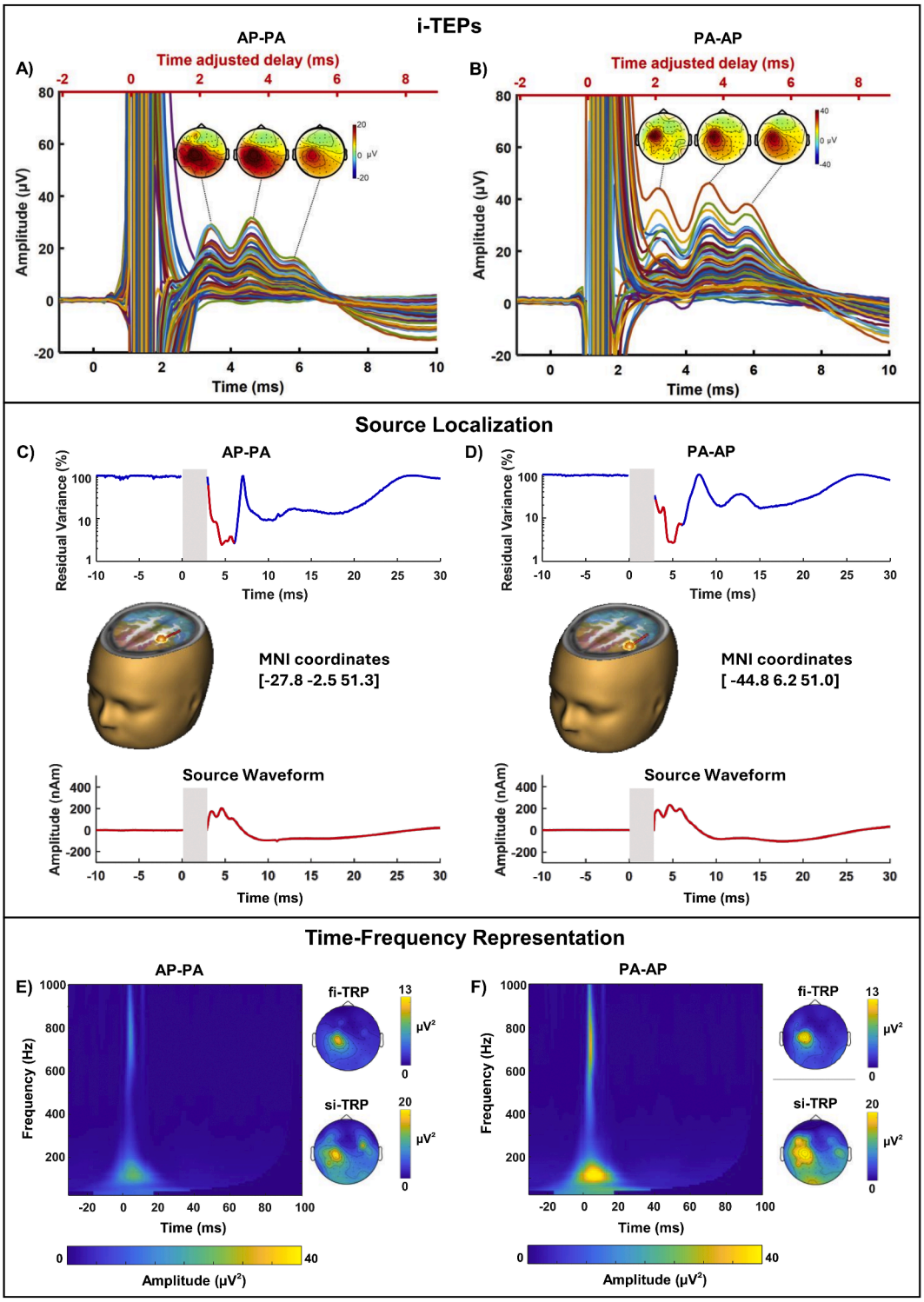

Fig. 1. Grand average across trials of the NoMuscle groups for the AP-PA (panels A, C, E) and PA-AP (B, C, D) conditions. The top panels (A, B) depict the i-TEPs and the topography at the three peaks; the TMS artifact was interpolated in the analyses and is shown here for display purposes. The red x-axis accounts for the Analog Signal Line Delay introduced by the amplifier, approximately 1.1 ms relative to the trigger. The middle panels (C, D) show the source localization of the dipole that best explains the signal recorded over the scalp. The bottom panels (E, F) show the i-TRP at channel C3 and the topographies at the two time–frequency windows of interest (amplitude range in color bars).

amplitudes exceeding 100 μV in the 50 ms before the TMS pulse, were rejected. Finally, the MEP amplitude in each trial was calculated as the difference between the highest and the lowest recorded voltage in the interval between 20 and 50 ms after TMS.

Only trials with both i-TEPs and MEPs were included in the final dataset: specifically, trials were removed if MEPs amplitude was lower than 50 μV (mean ± SE: 14.4 % ± 2.3 % in AP-PA, and 13 % ± 1.5 % in PA-AP) and/or if i-TEPs were contaminated by noise or artifacts, as specified in the i-TEPs preprocessing. Overall, the number of trials considered for each subject ranged between 46 and 68 for the AP-PA condition and between 46 and 78 for the PA-AP condition.

All the described preprocessing steps were performed in MATLAB (MathWorks, Natick, MA, USA) via EEGLAB (Delorme and Makeig, 2004) and Fieldtrip functions (Oostenveld et al., 2011).

2.1.6. Source localization

We used BESA Research (v. 7.1, BESA GmbH, Gräfelfing, Germany) to create a source model of the i-TEPs based on dipole fitting. The source model was computed separately for the AP-PA condition and for the PA-AP condition, using a standardized template head model (4 shell ellipsoidal). The procedure began by considering the grand average i-TEPs of the NoMuscle group in the interval between 2.8 and 6 ms from the TMS pulse. First, we placed one dipole within the head and let the algorithm identify the dipole location and orientation that yielded the lowest residual variance. Fitting the first dipole in the NoMuscle group optimized the signal-to-noise ratio during dipole fitting by reducing the presence of muscle artifacts superimposed on the signal of interest. The percentage of residual variance (RV) within the time window of interest (2.8–6 ms) was used as an estimate of the model's goodness of fit (Scherg and Ebersole, 1993). The selection of a single dipole to represent the data for the NoMuscle group was validated not only by the presence of low residual variance but also by a relatively flat residual signal (Scherg and Picton, 1991). Furthermore, the source waveform of the identified dipole exhibited the same three-peak characteristics as i-TEPs (Fig. 1). Once the dipole model was completed for the NoMuscle group, it was used as starting point to create the dipole model in the Muscle group. Again, the RV and a flat residual signal were considered to decide whether the model sufficiently explained the data or if it needed to include more dipoles.

For the groups with Muscle, a single dipole was insufficient to adequately reduce the residual variance below 20 % and flatten the residual signal. Therefore, we added a new dipole and let the algorithm identify its location and orientation. For the Muscle AP-PA condition, fitting two dipoles resulted in the residual variance below 20 % and a relatively flat residual signal. For the Muscle PA-AP condition, three dipoles were necessary (Figure S5).

Finally, we obtained the positions of the dipoles as MNI coordinates, the corresponding nearest anatomical structure and the associated Brodmann area.

2.1.7. Statistics

Statistics were run in the subgroup of subjects that had been included in the NoMuscle group for both the AP-PA and PA-AP conditions, in a within-subject design (8 subjects, 921 observations). Generalized mixed models with a gamma distribution and a log link function were used to test the relationship between single-trials i-TRP (as a fixed effect) and MEP amplitude (as the dependent variable), including the interaction between i-TRP and current direction. Subjects were included as a random effect, and the current direction (AP-PA, PA-AP) as a fixed effect. Trials were not included as a random effect, as a control analysis showed that its impact on the effects of interest was negligible, i.e., it did not substantially impact either residual variability or the estimate of fixed effects (results not shown). Separate models were run for fi-TRP and si-TRP. Moreover, generalized mixed models (gamma distribution, log link function) with subjects as a random effect were used to test for changes in i-TRP (fi-TRP and si-TRP as dependent variables in separate models) depending on the current direction (AP-PA, PA-AP; as fixed effects). Considering that separate models were run for the two current directions, significance level was adjusted according to Bonferroni correction ($\alpha/2 = 0.025$). To further assess the robustness of the relationship between i-TRP and MEP amplitude, we investigated the effects in an enlarged dataset of 14 subjects (794 observations), including participants of the NoMuscle group when considering the AP-PA condition only. Specifically, consistent with the main analyses, separate generalized mixed models with a gamma distribution and a log link function were run for fi-TRP and si-TRP (fixed effects), with MEP amplitude as the dependent variable. Subjects were included as a random effect.

Finally, post-hoc calculation of the power of the significant effects was performed via 1000 Monte Carlo simulations using the simr package in R (Green and Macleod, 2016).

The statistics were run in R v. 4.3.2 (R Core Team, 2021; packages 'lme4' for mixed-effects models (Bates et al., 2015 and 'emmeans' for post hoc comparisons, Lenth et al., 2024).

2.2. Conceptual validation

To further exclude the contribution of muscle artifact to i-TEPs, we ran a conceptual validation aimed at evoking cranial muscle responses without cortical stimulation by delivering TMS pulses over a lateral site corresponding to the temporal branch of the facial nerve at a very low intensity. We subsequently compared the obtained signal with i-TEPs obtained from the stimulation of the cortical motor hotspot (Fig. 3A).

TMS-EEG was acquired from three subjects from C3, and EMG signals were recorded from the right *first dorsal interosseous* via a bipolar belly tendon montage. For each condition, 100 single TMS pulses were delivered at random intervals with a figure-of-eight coil (Magstim model Alpha B.I. coil range, diameter: 70 mm). Recording settings were the same as the main experiment.

To obtain i-TEPs, TMS was delivered over the left primary motor cortex (M1) at 110 % of the resting motor threshold (rMT), with a 45-degree coil orientation to the medial−sagittal plane and AP−PA current direction. The rMT of the three subjects was equal to 59 % MSO (subj-01), 55 % MSO (subj-02) and 43 % MSO (subj-03).

To evoke cranial muscle twitches while minimizing cortical stimulation, we aimed to stimulate cranial nerves with low-intensity stimulation. This procedure is based on evidence that nerves are more excitable than muscles and that their stimulation can induce muscle contraction within a few ms (Purves-Stewart and Worster-Drought, 1952). Therefore, the TMS intensity was set at 10 % of the MSO, and the coil was moved laterally to C3. The nerve hotspot was defined as the location that evoked the largest muscle artifact in C3. The TMS intensity was increased from 5 % MSO to 10, 13, 15 and 18 % MSO or until a clear muscle artifact could be seen in C3.

The data were preprocessed to obtain i-TEPs and i-TRP over C3 via the same procedure used in the main experiment, except that the data were epoched from −50 ms to 50 ms. As in the main experiment, the reported latencies refer to the originally recorded signal, which includes the 1.1 ms delay relative to the actual onset of the TMS pulse.

3. Results

3.1. i-TEPs

Under both current direction conditions, a series of three peaks superposed to a positive slower potential was visible within the first 6 ms after TMS (Fig. 1A, B). The topographic distribution revealed a higher amplitude around the C3 electrode. These peaks were also visible in the averaged signal of single subjects, although with some variability (Figures S1 and S2), and even at the single-trial level in the NoMuscle group (Figures S3 and S4). Therefore, the recorded signal resembled the i-TEPs reported by Beck et al. (2024).

To understand the contribution of the TMS-induced muscle artifact, we also explored data from subjects among whom this artifact was visually detected (i.e., the Muscle group). In the AP-PA condition, the muscle artifact generally had a low amplitude, and the characteristic three peaks of i-TEPs were still visible both in the grand average (Figure S5A) and in all single-subject data (Figure S6). In the PA-AP condition, the muscle artifact had a stronger impact on the signal (Figures S5B and S7), possibly due to the higher stimulation intensity employed in this condition, which showed higher rMT (Beck et al., 2024; Guidali et al., 2023). Notably, this difference in rMT between PA-AP and AP-PA current directions has already been statistically demonstrated in (Guidali et al., 2023), where multiple coil orientations were directly compared (AP-PA, PA-AP, ML-LM). As reported in the Supplementary Figures of that paper, PA-AP stimulation consistently required higher rMT than AP-PA stimulation, supporting the interpretation provided here.

It should be noted that i-TEPs were not visible in the originally published paper (Guidali et al., 2023) possibly due to the preprocessing pipeline applied which included a low-pass filter and SSP-SIR algorithm, to attenuate high frequency components. For the sake of completeness, Figure S8 shows the overall TEPs (up to 350 ms) for the four conditions considered in this study, with the same preprocessing applied to i-TEPs.

3.2. Source localization

The time-varying cortical activity that explains the scalp i-TEPs is shown in Fig. 1C, D. The grand-average i-TEPs for the NoMuscle groups can be explained by a single dipole (Dip1) localized in the left precentral gyrus for both current directions, corresponding to Brodmann area 6 (MNI coordinates, AP-PA: −27.8, −2.5, 51.3; PA-AP: −44.8, 6.2, 51.0). The RVs of these models for the interval of interest were 8 % for AP-PA and 9 % for PA-AP, although higher RV values were present soon after the TMS pulse, possibly due to residual decay artifacts. Interestingly, the temporal pattern of the dipole activity showed three peaks characteristic of i-TEPs.

For Muscle groups, the source analysis resulted in two different models depending on the current direction. In the AP-PA condition (Figure S5), adding one more dipole (Dip2) to the source model was sufficient to obtain an RV of 13 % over the interval of interest. Dip2 was located outside the brain, on the lateral aspect of the head, just in front of the left ear (MNI coordinates: −67.5, 16.8, −42.7). The dipole was placed in line with muscles located on the lateral side of the head, such as the auricularis muscles or the temporalis muscle. Importantly, the time course of Dip2 activity resembled an M-wave (Di Bella et al., 1997), whereas the three peaks typical of i-TEPs were still visible in Dip1.

In the PA-AP condition (Figure S5), the muscle artifact was more prominent, and the model required 2 more dipoles (Dip2 and Dip3) to reach an RV below 20 %, i.e., 9 %. Dip2 was positioned again on the left side of the head, in front of the ear (MNI coordinates: −80.2, 7.9, −20.1). Dip3 was positioned between Dip1 and Dip2, outside the edge of the cortical surface (MNI coordinates: −68.3, 6.46, 22.9). The activity modeled by these two dipoles was strong and similar to that of muscle artifacts, whereas Dip1 seemed to involve less activity and faster oscillations.

3.3. Time-frequency analysis

The time−frequency analysis in the NoMuscle group revealed that in the activity within the first 10 ms post-stimulation, the ITC values are very high at approximately 700 Hz and between 100 and 200 Hz, suggesting a highly synchronized activity in the immediate TMS-EEG responses (Figure S9).

Moreover, we observed increased power after TMS in two frequency ranges for both the AP-PA and PA-AP conditions: between 100 and 200 Hz and between 600 and 800 Hz (Figure 1E, F). The topographies of both fi-TRP and si-TRP were centered around C3, qualitatively confirming a negligible or absent muscle artifact contamination.

3.4. Relationship with MEPs and current direction modulation

The generalized mixed model revealed that fi-TRP positively predicted MEP amplitude ($t = 3.2$, $p = 0.001$; estimated power: 88.8 %; 95 % CI: 86.7 %–90.7 %) such that the stronger the power in time-frequency range between 3–6 ms and 600–800 Hz, the greater the MEPs (Fig. 2A). Moreover, we found a significant effect of current direction, indicating that MEPs were higher in the AP-PA condition than in the PA-AP condition ($t = 2.7$, $p = 0.007$; estimated power: 77.8 %; 95 % CI: 75.1 %–80.3 %). No significant interaction between the fi-TRP and current direction was detected ($t = -0.8$, $p = 0.43$).

The same model including si-TRP (i.e., the power averaged between 3–6 ms and 100–200 Hz) as a predictor also revealed a positive relationship with MEPs ($t = 3.1$, $p = 0.002$; estimated power: 93.8 %; 95 % CI: 92.1 %–95.2 %); this relationship is likely explained by PA-AP, as revealed by the significant interaction between si-TRP and current direction ($t = -3.6$, $p < 0.001$; estimated power: 97.3 %; 95 % CI: 96.1 %, 98.2 %). Indeed, post hoc comparisons revealed a significant positive relationship between si-TRP power and MEP amplitude in the PA-AP condition ($p = .002$) but not in the AP-PA condition ($p = 0.09$; Fig. 2C). The effect of the current direction on MEPs was confirmed ($t = 4.3$, $p < 0.001$; estimated power: 99.4 %; 95 % CI: 98.7 %, 99.8 %).

Results from the enlarged sample including all the 14 subjects from the NoMuscle AP-PA group confirmed that MEP amplitude was significantly predicted by fi-TRP ($t = 2.9$, $p = 0.004$; estimated power: 79 %; 95 % CI: 76.3 %−81.5 %) but not by si-TRP ($t = 0.5$, $p = 0.623$).

Finally, both fi-TRP ($t = -19.8$, $p < 0.001$) and si-TRP ($t = -7.5$, $p < 0.001$) were modulated by current direction and were higher in the PA-AP condition than in the AP-PA condition (Fig. 2B–D).

3.5. Conceptual validation

In every subject, the stimulation of the motor hotspot at 110 % of the rMT resulted in visible i-TEPs in C3, with amplitude and latency in line with the data reported in the main experiment. Fig. 3 shows the result from a single subject (subj-01), while the remaining two (subj-02, subj-03) are reported in Supplementary Figures S10 and S11. The stimulation of the nerve hotspot was located approximately over FT7. Stimulations at 10–15 % MSO and above evoked a visible cranial muscle twitch that increased with increasing stimulation intensity (Fig. 3B). Although nerve stimulation may evoke a muscle twitch of similar amplitude of i-TEPs (at 13 % MSO for subj-01 – Fig. 3B – and subj-02 – Figure S10; at 15 % for subj-03 – Figure S11), the former did not present the high-frequency peaks typical of i-TEPs. While M1 stimulation presented a power increase in the two frequency ranges reported in the main experiment, i.e., 600–800 Hz and 100–200 Hz, nerve stimulation was associated with a power increase in the range of 100–200 Hz at lower intensities (Fig. 3C). Importantly, when nerve stimulation induced a muscle twitch had an amplitude similar to that of i-TEPs, the power was increased at frequencies ranging from 100 to 400 Hz. To ensure comparable response amplitude across conditions within the 3–6 ms window for subj-02 and subj-03 we adopted an offline trial-matching procedure that iteratively excluded extreme trials. As shown in the updated Figures S10 and S11 (lower inset, left panel), this adjustment resulted in comparable signal amplitudes in the time domain for both subjects.

4. Discussion

Our study confirmed the presence of i-TEPs within the first 6 ms after stimulation, characterized by three peaks with a topographical distribution over centrolateral electrodes surrounding the M1 hotspot, for both the AP-PA and PA-AP current directions. Most importantly, our results suggest that the activity recorded in the i-TEPs window contains a physiological response representing the neuronal excitability of the

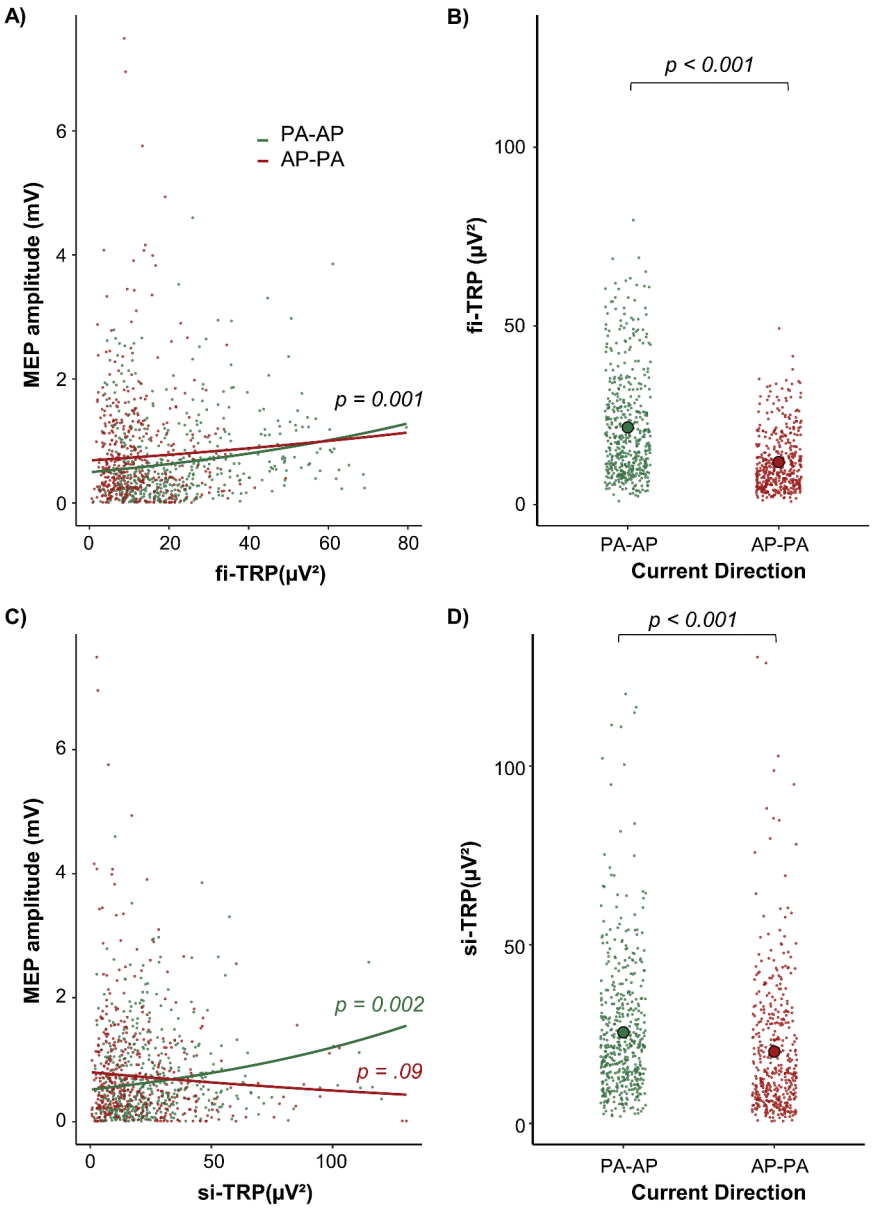

Fig. 2. Relationship with MEPs and current direction modulation for fi-TRP (A and B, respectively) and si-TRP (C and D, respectively). Dots represent single trial values. The fitted lines in A represent the main effect of fi-TRP along with the absence of interaction between fi-TRP and the current direction, whereas those in C reflect the interaction effect between si-TRP and the current direction, with only PA-AP showing a significant positive relationship with the MEP amplitude. The large dots in B and D indicate the average i-TRP concentration across trials.

stimulated motor cortex. Despite it cannot fully ruled out that this activity is partly contaminated by residual artifacts, e.g. mechanical or muscle artifacts, this study shows evidence that the immediate TMS-EEG response can be informative on motor cortex excitability. First, we found a positive association between i-TRP and the amplitude of MEPs. Second, source localization models indicated that i-TEPs are generated in the precentral gyrus of the stimulated hemisphere and that their activity can be clearly distinguished from sources of muscle twitches. Finally, the conceptual validation suggested that immediate TMS-EEG responses do not reflect muscle artifacts, as evidenced by the distinct pattern compared with muscle twitches.

To understand the physiological origin of the activity recorded immediately after TMS, we considered both phase-locked activity, i.e., i-TEPs, and the total oscillatory response, i.e., i-TRP, which comprises both phase-locked (i.e., evoked) and non-phase-locked (i.e., induced) activity (Herrmann et al., 2014 Kalcher and Pfurtscheller, 1995). Nevertheless, our data suggest that phase-locked activity is stronger than induced oscillations and that i-TRP mainly represents i-TEPs, as i-TEPs are visible as strong phase-locked activity at the single-trial level in all subjects and the ITC shows high values within the first 10 ms after the TMS pulse. This finding is in line with previous evidence that TMS induces a short-lasting phase reset of ongoing oscillations (Herring et al., 2015; Romei et al., 2010; Romei et al., 2011).

Importantly, time–frequency analysis allowed us to disentangle the contribution of faster and slower components of i-TEPs both in terms of the relationship with MEP amplitude and in the comparison between current directions. Time–frequency analysis revealed two clusters of increased power after TMS in the ranges between 600 and 800 Hz and between 100 and 200 Hz in the first ms after the TMS pulse on the electrode closest to the stimulation site.

The fast frequencies discussed here lie well beyond the range typically considered physiological for scalp EEG. However, substantial evidence indicates that bursts of very high-frequency activity—ranging from 600 Hz to 1 kHz—can indeed be detected in scalp EEG under

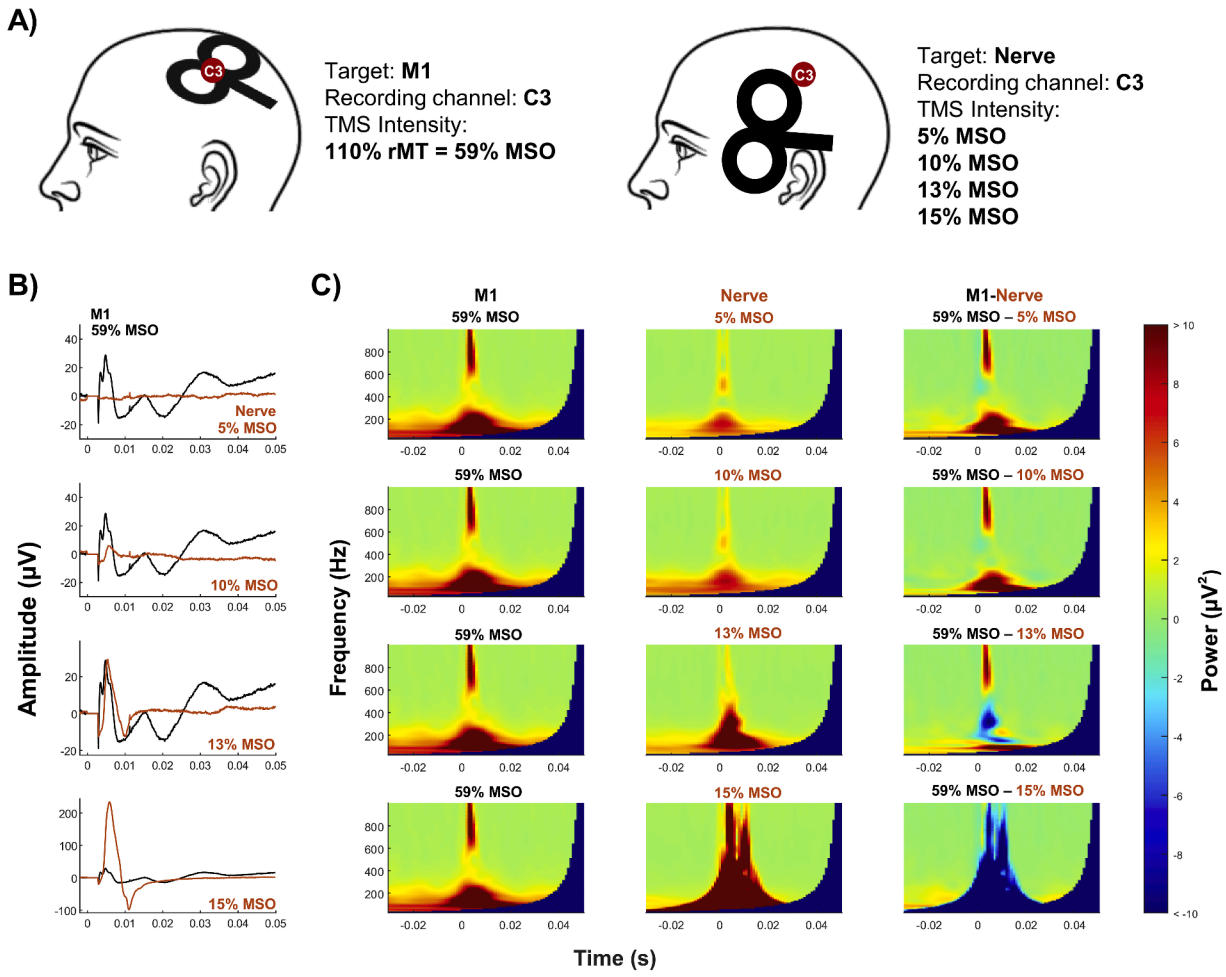

Fig. 3. Conceptual validation with results from a representative subject (subj-01). A) Schematic representation of the two stimulation conditions, which target the M1 hotspot (left) and the cranial nerve (right). B) Average TEPs recorded after M1 stimulation at 110 % of the rMT (black trace) overlapped with those recorded after nerve stimulation (orange trace), with increasing intensity from the top to the bottom row (i.e., 5, 10, 13 and 15 % of the MSO). C) Time-frequency representation of the signal recorded in C3 after M1 stimulation at 110 % rMT (left column), after nerve stimulation with increasing intensity from the top row to the bottom row (middle column) and the difference between the two (right column). Power range in color bar.

specific conditions, such as following electrical stimulation of the median nerve (Fedele et al., 2012). It has been suggested that these 600 Hz components in EEG and MEG, called sigma-burst, may reflect neuronal spiking activity (Curio et al., 1994). Supporting this hypothesis, simultaneous recordings in awake macaque monkeys have shown that macroscopic high-frequency EEG bursts around 600 Hz coincide with synchronized spike bursts of neurons in the primary somatosensory cortex, as revealed by invasive single-cell micro-recordings (Baker et al., 2003). Regarding the motor system, the fast frequencies we detected align with the estimated relevant frequencies for I-waves (Di Lazzaro et al., 2012; Ziemann and Rothwell, 2000) and with spike bursts generated by fast pyramidal tract neurons in the sensorimotor cortex, which fire with an interspike interval of approximately 1.5–2.5 ms (Calvin and Sypert, 1976; Curio, 2000). Although EEG is generally more sensitive to postsynaptic potentials (Da Silva, 2010), the strong neuronal synchronization induced by TMS at immediate latencies (Di Lazzaro et al., 1998) may allow these spike bursts to be detected at the scalp level. Nonetheless, further research is needed to clarify the mechanisms underlying the generation of this high-frequency response.

On the other hand, the slower frequencies fall within the “ripples” range. These oscillations have been observed in healthy brains in several brain regions, including sensorimotor areas of the neocortex, and in several cognitive states (Gerner et al., 2020; Matsumoto et al., 2013) . Thus, the TMS coils act as an external stimulus, inducing activity that is physiologically plausible in the target area. So, differently from the fi-TRP components that we, as Beck and colleagues, interpreted as reflecting the fast and repetitive activity of action potentials volleys, we speculate that the physiological mechanisms underlying the si-TRP, is a TMS-evoked hypersynchronization of intracortical postsynaptic potentials.

If the activity recorded in the cortex is a precursor of I-waves in the corticospinal tract and then MEPs in the muscles, it should be a) present in both current directions and b) associated with MEPs in both current directions. Although the former is true for both si-TRP and fi-TRP, the latter was verified for fi-TRP only, as the relationship between si-TRP and MEPs was significant for the PA-AP condition only. Considering that ripple generation involves activity in larger neural populations than very fast ripples, it is possible that a larger network is more affected by changes in current directions. Alternatively, this frequency range may be more prone to the influence of concomitant muscle artifacts (Barchiesi et al., 2020). However, more studies are needed to understand the functional meaning of the si-TRP that we identified in this study.

Furthermore, both fi-TRP and si-TRP are modulated by the current direction such that PA-AP is stronger than AP-PA. This finding is in line with the findings of Beck and colleagues on the amplitude of i-TEPs peaks 2 and 3 when adjusting the TMS intensity on the rMT of the respective current directions. On the other hand, the MEP amplitude was

higher for the AP-PA condition than for the PA-AP condition. To the best of our knowledge, no previous study reported a direct statistical comparison of MEP amplitude for AP-PA and PA-AP current direction for biphasic pulses (but see: Sommer et al., 2006; Sommer et al., 2018)). A possible explanation for the higher MEP amplitude in AP-PA stimulation is that this current direction is more effective in activating pyramidal neurons projecting into the cortico-spinal tract (Calvin and Sypert, 1976), and that the input-output curve for the two directions does not grow with similar gain as intensity increases. However, this explanation is speculative and more studies need to be performed in the future to address this specific issue.

Other evidence that immediate TMS-related activity has a cortical origin and is evoked in the area around the site of stimulation comes from the source localization of i-TEPs. While the topographic maps showed a dipolar pattern consistent with activation over the sensorimotor cortex, source analysis offered a more systematic and anatomically informed estimate of the underlying generators within the precentral gyrus, reducing reliance on subjective visual interpretation and allowing extraction of source waveforms for further validation. This approach was further supported by the presence of clean data (i.e., for NoMuscle case), a clear topographic pattern suggestive of a single dominant source, and strong a priori anatomical constraints, all of which are known to improve the reliability of dipole fitting (Cuffin et al., 1991; Leahy et al., 1998). The dipole explaining cortical activation in cases with no muscular response maintained the characteristic three peaks unfolding in the first 3 ms of the recovered signal, and this feature was also clearly visible in the AP-PA condition, in which the muscle artifact was of relatively low amplitude. Notably, the source localization models clearly distinguished between the generator of the i-TEPs and generators of muscle twitches.

Finally, the conceptual validation provided further evidence that muscular activity is unlikely to be at the origin of i-TEPs and i-TRP. The stimulation of a lateral site corresponding with the temporal branch of the facial nerve started to evoke a clear muscular response on C3 even at very low TMS intensity, approximately 19 % of the rMT. At this extremely low intensity, it is improbable that the underlying cortex was directly stimulated by TMS. If i-TEPs were contaminated by muscular artifacts, we would expect a similar pattern when the stimulation targeted a cranial nerve. While comparable in amplitude in the first 10 ms after the TMS pulse, the signals recorded from M1 and nerve stimulation showed marked differences both in the time domain and in the time–frequency pattern. Indeed, the three peaks characteristic of i-TEPs, clearly present after M1 stimulation, were absent after nerve stimulation. Consistently, the i-TRP showed increased activity mostly at frequencies below 500 Hz.

On the other hand, it is important to consider that muscle artifacts remain a major obstacle for recording immediate TMS-EEG responses. In our study, of the 28 participants included in the original dataset, only half of them showed no muscle activity in the TEPs recorded in the AP-PA condition, and even fewer showed no muscle activity in the PA-AP condition (10/28). This proportion of clean/rejected recordings highlights that obtaining large datasets and high statistical power is challenging and costly with current state-of-the-art procedures. While online correction methods for coil tilting have been suggested (Casarotto et al., 2022), the muscle is not an all-or-nothing type of response, and optimized stimulation can still result in subtle muscle twitches that are difficult to spot. It is possible that the i-TEPs very high amplitude, i.e., 2–5 times higher than typical TEPs, may be the result of the superposition of the cortical response with very small residual of muscle artifact, although topographic maps from the current work and from Beck et al. (2024) suggest that this putative contribution is minimal.

Overall, our findings converge in indicating immediate TMS-EEG responses as an excitability index of the stimulated motor cortex, ruling out the potential contribution of muscle artifacts. Importantly, immediate TMS-EEG responses seem to contain two separate responses with distinct functional meanings. It is possible that fi-TRP is linked to the activity of neurons composing the corticospinal tract and to the I-waves, eventually leading to MEPs. Differently, si-TRP does not seem to be consistently related to the corticospinal tract and does not resemble the characteristic features of I-waves. Future studies are needed to understand what si-TRP represents. That said, it is important to acknowledge that immediate TMS-EEG responses are likely to originate in the motor cortex, as shown by the results of the source localization in this study. This finding aligns with previous double-pulse stimulation studies indicating that the generation of I-waves arises from a local cortical circuit of inhibitory interneurons and excitatory neurons (Ziemann, 2020). Therefore, immediate TMS-EEG responses should not be influenced by processes occurring at the synaptic station between upper motor neurons and the spinal cord, unlike MEPs. Nevertheless, given the novelty of the phenomenon, future research will be needed to assess the replicability and generalizability of the present results. These results have significant implications across both basic research and clinical settings. Specifically, immediate TMS-EEG responses may be used to explore the role of M1 in neurophysiological processes associated with movement representation, including aspects such as action intention and movement awareness. Furthermore, as noninvasive indicators unaffected by spinal activity, i-TEPs and i-TRP from M1 stimulation present a promising, easily obtainable biomarker for diagnosing motor disorders and neuropsychiatric conditions linked to cortical excitability changes, as well as for monitoring the effectiveness of therapeutic interventions.

Funding

A.S., A.Z., N.B., E.D. and M.B. were supported by the Italian Ministry of Health ‘Ricerca Corrente’; G.B. was funded by the Department of Philosophy ‘Piero Martinetti’ of the University of Milan with the Project “Departments of Excellence 2023–2027” awarded by the Italian Ministry of Education, University and Research (MIUR) and by the PRIN 2022 grant (2022SP5K99, Italian Ministry of Education, University and Research (MIUR)).

Data and code availability statement

The raw data are available at the following link: https://gin.g-node.org/Giacomo_Guidali/Guidali_et_al_2023_EJN_RR.

CRediT authorship contribution statement

Antonietta Stango: Writing – review & editing, Visualization, Methodology, Investigation, Formal analysis, Data curation, Conceptualization. **Agnese Zazio:** Writing – original draft, Visualization, Methodology, Investigation, Formal analysis, Conceptualization. **Guido Barchiesi:** Writing – review & editing, Visualization, Methodology, Formal analysis, Conceptualization. **Natale Salvatore Bonfiglio:** Writing – review & editing, Formal analysis. **Elisa Dognini:** Writing – review & editing, Formal analysis. **Eleonora Marcantoni:** Writing – review & editing, Formal analysis. **Marta Bortoletto:** Writing – original draft, Validation, Supervision, Project administration, Methodology, Conceptualization.

Declaration of competing interest

The authors declare that they have no conflicts of interest.

Acknowledgment

We acknowledge the use of publicly available data from https://gin.g-node.org/Giacomo_Guidali/Guidali_et_al_2023_EJN_RR provided by Giacomo Guidali and Delia Lucarelli.

Supplementary materials

Supplementary material associated with this article can be found, in the online version, at doi:10.1016/j.neuroimage.2025.121666.

References

Almeida, P.R., Vieira, J.B., Silveira, C., Ferreira-Santos, F., Chaves, P.L., Barbosa, F., et al., 2011. Exploring the dynamics of P300 amplitude in patients with schizophrenia. Int. J. Psychophysiol. 81, 159–168. https://doi.org/10.1016/j.ijpsycho.2011.06.006.

Baker, S.N., Curio, G., Lemon, R.N., 2003. EEG oscillations at 600 Hz are macroscopic markers for cortical spike bursts. J. Physiol. 550 (2), 529–534. https://doi.org/10.1113/jphysiol.2003.045674.

Barchiesi, G., Demarchi, G., Wilhelm, F.H., Hauswald, A., Sanchez, G., Weisz, N., 2020. Head magnetomyography (hMMG): A novel approach to monitor face and whole head muscular activity. Psychophysiol. 57 (3), 1–13. https://doi.org/10.1111/psyp.13507.

Bates, D., Mächler, M., Bolker, B.M., Walker, S.C., 2015. Fitting linear mixed-effects models using lme4. J. Stat. Softw. 67. https://doi.org/10.18637/jss.v067.i01.

Beck, M.M., Christiansen, L., Madsen, M.A.J., Jadidi, A.F., Vinding, M.C., Thielscher, A., Tomasevic, L., 2024. Transcranial magnetic stimulation of primary motor cortex elicits an immediate transcranial evoked potential. Brain Stimul. 17 (4), 802–812. https://doi.org/10.1016/j.brs.2024.06.008.

Bergmann, T.O., Hartwigsen, G., 2021. Inferring causality from noninvasive brain stimulation in cognitive neuroscience. J. Cogn. Neurosci. 33, 195–225. https://doi.org/10.1162/jocn_a_01591.

Bortoletto, M., Veniero, D., Thut, G., Miniussi, C., 2015. The contribution of TMS – EEG coregistration in the exploration of the human cortical connectome. Neurosci. Biobehav. Rev. 49, 114–124. https://doi.org/10.1016/j.neubiorev.2014.12.014.

Burke, D., Hicks, R., Gandevia, S.C., Stephen, J., Woodforth, I., Crawford, M., 1993. Direct comparison of corticospinal volleys in human subjects to transcranial magnetic and electrical stimulation. J. Physiol. 470, 383–393. https://doi.org/10.1113/jphysiol.1993.sp019864.

Calvin, W.H., Sypert, G.W., 1976. Fast and slow pyramidal tract neurons: an intracellular analysis of their contrasting repetitive firing properties in the cat. J. Neurophysiol. 39 (2), 420–434. https://doi.org/10.1152/jn.1976.39.2.420.

Casarotto, S., Fecchio, M., Rosanova, M., Varone, G., D'Ambrosio, S., Sarasso, S., et al., 2022. The rt-TEP tool: real-time visualization of TMS-Evoked Potentials to maximize cortical activation and minimize artifacts. J. Neurosci. Methods 370, 109486. https://doi.org/10.1016/j.jneumeth.2022.109486.

Cohen, M.X., van Gaal, S., 2014. Subthreshold muscle twitches dissociate oscillatory neural signatures of conflicts from errors. Neuroimage 86, 503–513. https://doi.org/10.1016/j.neuroimage.2013.10.033.

Cuffin, B.N., Cohen, D., Yunokuchi, K., Maniewski, R., Purcell, C., Cosgrove, G.R., Schomer, D., 1991. Tests of EEG localization accuracy using implanted sources in the human brain. Annal. Neurol. 29 (2), 132–138. https://doi.org/10.1002/ana.410290204.

Curio, Gabriel, Mackert, B.M., Burghoff, M., Koetitz, R., Abraham-Fuchs, K., Härer, W., 1994. Localization of evoked neuromagnetic 600 Hz activity in the cerebral somatosensory system. Electroencephal. Clin. Neurophysiol. 91 (6), 483–487. https://doi.org/10.1016/0013-4694(94)90169-4.

Curio, G., 2000. Linking 600-Hz "spikelike" EEG/MEG wavelets ("sigma-bursts") to cellular substrates: concepts and caveats. J Clin Neurophysiol 17 (4), 377–396. https://doi.org/10.1097/00004691-200007000-00004.

Da Silva, F.L., 2010. EEG: Origin and measurement. In: *EEG - fMRI*, pp. 23–48. https://doi.org/10.1007/978-3-540-87919-0_2.

Delorme, A., Makeig, S., 2004. EEGLAB: an open source toolbox for analysis of single-trial EEG dynamics including independent component analysis. J. Neurosci. Methods 134, 9–21. https://doi.org/10.1016/j.jneumeth.2003.10.009.

Di Bella, P., Logullo, F., Lagalla, G., Sirolla, C., Provinciali, L., 1997. Reproducibility of normal facial motor nerve conduction studies and their relevance in the electrophysiological assessment of peripheral facial paralysis. Neurophysiol. Clin. 27, 300–308. https://doi.org/10.1016/S0987-7053(97)85828-5.

Di Lazzaro, V., Oliviero, A., Profice, P., Saturno, E., Pilato, F., Insola, A., Rothwell, J.C., 1998. Comparison of descending volleys evoked by transcranial magnetic and electric stimulation in conscious humans. Electroencephal.Clin.Neurophysiol. - Electromyo. Motor Control 109 (5), 397–401. https://doi.org/10.1016/S0924-980X(98)00038-1.

Di Lazzaro, V., Oliviero, A., Profice, P., Insola, A., Mazzone, P., Tonali, P., et al., 1999. Effects of voluntary contraction on descending volleys evoked by transcranial electrical stimulation over the motor cortex hand area in conscious humans. Exp. Brain Res. 124, 525–528. https://doi.org/10.1007/s002210050649.

Di Lazzaro, V., Oliviero, A., Mazzone, P., Insola, A., Pilato, E., Saturno, E., et al., 2001. Comparison of descending volleys evoked by monophasic and biphasic magnetic stimulation of the motor cortex in conscious humans. Exp. Brain Res. 141, 121–127. https://doi.org/10.1007/s002210100863.

Di Lazzaro, V., Profice, P., Ranieri, F., Capone, F., Dileone, M., Oliviero, A., Pilato, F., 2012. I-wave origin and modulation. Brain Stimul. 5 (4), 512–525. https://doi.org/10.1016/j.brs.2011.07.008.

Farzan, F., 2024. Transcranial magnetic stimulation–electroencephalography for biomarker discovery in psychiatry. Biol. Psychiatry 95, 564–580. https://doi.org/10.1016/j.biopsych.2023.12.018.

Fedele, T., Scheer, H.J., Waterstraat, G., Telenczuk, B., Burghoff, M., Curio, G., 2012. Towards non-invasive multi-unit spike recordings: Mapping 1kHz EEG signals over human somatosensory cortex. Clin. Neurophysiol. 123 (12), 2370–2376. https://doi.org/10.1016/j.clinph.2012.04.028.

Freche D., Naim-Feil J., Peled A., Levit-Binnun N., Moses E. A quantitative physical model of the TMS-induced discharge artifacts in EEG. vol. 14. 2018. 10.1371/journal.pcbi.1006177.

Gerner, N., Thomschewski, A., Marcu, A., Trinka, E., Höller, Y., 2020. Pitfalls in Scalp High-Frequency Oscillation Detection From Long-Term EEG Monitoring. Front. Neurol. 11. https://doi.org/10.3389/fneur.2020.00432.

Green, P., Macleod, C.J., 2016. SIMR: an R package for power analysis of generalized linear mixed models by simulation. Methods Ecol. Evol. 7, 493–498. https://doi.org/10.1111/2041-210X.12504.

Guidali, G., Zazio, A., Lucarelli, D., Marcantoni, E., Stango, A., Barchiesi, G., Bortoletto, M., 2023. Effects of transcranial magnetic stimulation (TMS) current direction and pulse waveform on cortico-cortical connectivity : a registered report TMS-EEG study. Eur. J. Neurosci. 58, 3785–3809. https://doi.org/10.1111/ejn.16127.

Hernandez-Pavon, J.C., Veniero, D., Bergmann, T.O., Belardinelli, P., Bortoletto, M., Casarotto, S., et al., 2023. TMS combined with EEG: recommendations and open issues for data collection and analysis. Brain Stimul. 16, 567–593. https://doi.org/10.1016/j.brs.2023.02.009.

Herring, J.D., Thut, G., Jensen, O., Bergmann, T.O., 2015. Attention modulates TMS-locked alpha oscillations in the visual cortex. J. Neurosci. 35, 14435–14447. https://doi.org/10.1523/JNEUROSCI.1833-15.2015.

Herrmann, C.S., Rach, S., Vosskuhl, J., Strüber, D., 2014. Time-frequency analysis of event-related potentials: a brief tutorial. Brain Topogr. 27, 438–450. https://doi.org/10.1007/s10548-013-0327-5.

Ilmoniemi, R.J., Virtanen, C.A.J., Ruohonen, J., Karhu, J., Aronen, H.J., Näätänen, R., et al., 1997. Neuronal responses to magnetic stimulation reveal cortical reactivityand connectivity. Neuroreport 8, 3537–3540.

Kalcher, J., Pfurtscheller, G., 1995. Discrimination between phase-locked and non-phase-locked event-related EEG activity. Electroencephalogr. Clin. Neurophysiol. 94, 381–384. https://doi.org/10.1016/0013-4694(95)00040-6.

Kaneko, K., Kawai, S., Fuchigami, Y., Shiraishi, G., Ito, T., 1996. Effect of stimulus intensity and voluntary contraction on corticospinal potentials following transcranial magnetic stimulation. J. Neurol. Sci. 139, 131–136. https://doi.org/10.1016/0022-510X(96)00050-0.

Leahy, R.M., Mosher, J.C., Spencer, M.E., Huang, M.X., Lewine, J.D., 1998. A study of dipole localization accuracy for MEG and EEG using a human skull phantom. Electroencephal. Clin. Neurophysiol. 107 (2), 159–173. https://doi.org/10.1016/S0013-4694(98)00057-1.

Lenth R.V., Bolker B., Buerkner P., Giné-vázquez I., Herve M., Love J., et al. Package ' emmeans'. Https://CRANR-ProjectOrg/Package=emmeans 2024. 10.1080/00031305.1980.10483031>.License.

Massimini, M., Ferrarelli, F., Huber, R., Esser, S.K., Singh, H., Tononi, G., 2005. Breakdown of cortical effective connectivity during sleep. Science (80-) 309, 2228–2232. https://doi.org/10.1126/science.1117256.

Matsumoto, A., Brinkmann, B.H., Stead, S.M., Matsumoto, J., Kucewicz, M.T., Marsh, W. R., Worrell, G., 2013. Pathological and physiological high-frequency oscillations in focal human epilepsy. J. Neurophysiol. 110 (8), 1958–1964. https://doi.org/10.1152/jn.00341.2013.

Momi, D., Ozdemir, R.A., Tadayon, E., Boucher, P., Shafi, M.M., Pascual-Leone, A., et al., 2021. Network-level macroscale structural connectivity predicts propagation of transcranial magnetic stimulation. Neuroimage 229, 117698. https://doi.org/10.1016/j.neuroimage.2020.117698.

Momi, D., Wang, Z., Griffiths, J.D., 2023. TMS-evoked responses are driven by recurrent large-scale network dynamics. ELife 12, 1–33. https://doi.org/10.7554/eLife.83232.

Numssen O., Kuhnke P., Weise K., Hartwigsen G. Electric- - field- - based dosing for TMS 2024;2. 10.1162/imag.

Oostenveld, R., Fries, P., Maris, E., Schoffelen, J.M, 2011. FieldTrip: open source software for advanced analysis of MEG, EEG, and invasive electrophysiological data. Comput. Intell. Neurosci. 2011. https://doi.org/10.1155/2011/156869.

Ozdemir, R.A., Tadayon, E., Boucher, P., Momi, D., Karakhanyan, K.A., Fox, M.D., et al., 2020. Individualized perturbation of the human connectome reveals reproducible biomarkers of network dynamics relevant to cognition. Proc. Natl. Acad. Sci. U. S. A. 117, 8115–8125. https://doi.org/10.1073/pnas.1911240117.

Purves-Stewart, J., Worster-Drought, C., 1952. The Diagnosis of Nervous Diseases. Arnold.

Romei, V., Gross, J., Thut, G., 2010. On the role of prestimulus alpha rhythms over occipito-parietal areas in visual input regulation: correlation or causation? J. Neurosci. 30, 8692–8697. https://doi.org/10.1523/JNEUROSCI.0160-10.2010.

Romei, V., Driver, J., Schyns, P.G., Thut, G., 2011. Rhythmic TMS over parietal cortex links distinct brain frequencies to global versus local visual processing. Curr. Biol. 21, 334–337. https://doi.org/10.1016/j.cub.2011.01.035.

Rosanova, M., Casali, A.G., Bellina, V., Resta, F., Mariotti, M., Massimini, M., 2009. Natural frequencies of human corticothalamic circuits. J. Neurosci. 29, 7679–7685. https://doi.org/10.1523/JNEUROSCI.0445-09.2009.

Scherg, M., Ebersole, J.S., 1993. Models of brain sources. Brain Topogr. 5, 419–423. https://doi.org/10.1007/BF01128700.

Scherg, M., Picton, T.W., 1991. Separation and identification of event-related potential components by brain electric source analysis. Electroencephalogr. Clin. Neurophysiol. Suppl. 42, 24–37.

Sommer, M., Alfaro, A., Rummel, M., Speck, S., Lang, N., Tings, T., Paulus, W., 2006. Half sine, monophasic and biphasic transcranial magnetic stimulation of the human

motor cortex. Clin. Neurophysiol. 117 (4), 838–844. https://doi.org/10.1016/j.clinph.2005.10.029.

Sommer, M., Ciocca, M., Chieffo, R., Hammond, P., Neef, A., Paulus, W., Hannah, R., 2018. TMS of primary motor cortex with a biphasic pulse activates two independent sets of excitable neurones. Brain Stimul. 11 (3), 558–565. https://doi.org/10.1016/j.brs.2018.01.001.

Stango, A., Zazio, A., Barchiesi, G., Salvatore, N., Bortoletto, M., 2025. Impact of high-frequency sampling rate and stimulation intensity on early TMS artifacts: considerations for immediate TMS-EEG responses. Neuroimage 321, 121526. https://doi.org/10.1016/j.neuroimage.2025.121526.

Tremblay, S., Rogasch, N.C., Premoli, I., Blumberger, D.M., Casarotto, S., Chen, R., et al., 2019. Clinical utility and prospective of TMS–EEG. Clin. Neurophysiol. 130, 802–844. https://doi.org/10.1016/j.clinph.2019.01.001.

Veniero, D., Bortoletto, M., Miniussi, C., 2009. TMS-EEG co-registration : on TMS-induced artifact. Clin. Neurophysiol. 120, 1392–1399. https://doi.org/10.1016/j.clinph.2009.04.023.

Zazio, A., Barchiesi, G., Ferrari, C., Marcantoni, E., Bortoletto, M., 2022. M1-P15 as a cortical marker for transcallosal inhibition: a preregistered TMS-EEG study. Front. Hum. Neurosci. 16.

Ziemann, U., Rothwell, J.C., 2000. I-waves in motor cortex. J. Clin. Neurophysiol. 17 (4), 397–405. https://doi.org/10.1097/00004691-200007000-00005.

Ziemann, U., 2020. I-waves in motor cortex revisited. Exp. Brain Res. 238, 1601–1610. https://doi.org/10.1007/s00221-020-05764-4.